



## Original Article

# Establishment of a rat model of severe spontaneous intracerebral hemorrhage

Shuixiang Deng<sup>1,#</sup>, Shengjie Feng<sup>1,#</sup>, Yuewen Xin<sup>1</sup>, Yu He<sup>1</sup>, Yao Wang<sup>1</sup>, Mi Tian<sup>1,\*</sup>, Ye Gong<sup>1,2,\*</sup>

<sup>1</sup> Department of Critical Care Medicine, Huashan Hospital, Fudan University, Shanghai, China

<sup>2</sup> Department of Neurosurgery, Huashan Hospital, Fudan University, Shanghai, China



## ARTICLE INFO

Managing Editor: Jingling Bao

## Keywords:

Severe spontaneous intracerebral hemorrhage

Animal model

Autologous blood injection

Animal behavior

Lung injury

## ABSTRACT

**Background:** Severe intracerebral hemorrhage (ICH) is the most devastating subtype of stroke resulting in high mortality and disability. At present, the development of targeted treatments to minimize the high morbidity and mortality is limited partly due to the lack of a severe ICH animal model. In this study, we aimed to establish an accurate severe ICH model in rats and examine the pathological and physiological changes associated with ICH.

**Methods:** A rat model of severe ICH model was established by intrastriatal injection of autologous blood using different blood volumes (ICH 100  $\mu$ L group, ICH 130  $\mu$ L group, ICH 160  $\mu$ L group, ICH 170  $\mu$ L group, and ICH 180  $\mu$ L group). The mortality was assessed during the 28-day post-ICH period. Short- and long-term neurological deficits were evaluated using the Longa method, foot fault, falling latency, and Morris water maze tests. Brain water content, hematoma volume, hemoglobin content, and magnetic resonance imaging were assessed to determine the extent of brain injury. Immunofluorescence staining was conducted to examine microglial activation and neuronal apoptosis. Hematoxylin and eosin (H&E) staining, lung water content, and western blotting were used to assess lung injury following ICH.

**Results:** The mortality of ICH rats increased significantly with an increase in autologous blood injection. The 28-day mortality in the 100  $\mu$ L, 130  $\mu$ L, 160  $\mu$ L, 170  $\mu$ L, and 180  $\mu$ L ICH groups were 5%, 20%, 40%, 75%, and 100%, respectively. A significantly higher 28-day mortality was observed in the ICH 160  $\mu$ L group compared to the ICH 100  $\mu$ L group. The ICH 160  $\mu$ L group exhibited significantly increased neurological deficits, brain edema, hematoma volume, and hemoglobin content compared to the sham group. Compared with the sham operation group, the activation of microglia and neuronal death in ICH 160  $\mu$ L rats increased. The use of H&E staining and western blotting demonstrated that disruption of the intra-alveolar structure, alveolar edema, and infiltration of inflammatory cells and cytokines into the lung tissue were more severe in the ICH 160  $\mu$ L group than the sham group.

**Conclusions:** A severe ICH model in rats was successfully established using an injection of autologous blood at a volume of 160  $\mu$ L. This model may provide a valuable tool to examine the pathological mechanisms and potential therapeutic interventions of severe ICH.

## Introduction

According to the 2021 spontaneous intracerebral hemorrhage (ICH) Global Burden of Disease study, ICH accounts for about 15.0%–27.9% of all strokes, and has the highest mortality rate among all stroke types.<sup>[1,2]</sup> Several studies have reported that the 30-day mortality rate of ICH reached 30%–

55%.<sup>[3,4]</sup> The ICH syndrome usually occurs in the basal ganglia region,<sup>[5,6]</sup> which is mainly responsible for the regulation of body movement and sensation, so patients with severe ICH have a high rate of disability, which seriously affects the patient's motor and sensory functions.<sup>[7,8]</sup> An observational study of long-term outcomes in patients with ICH demonstrated a 6-month disability rate of up to 80%.<sup>[9]</sup> Therefore, it is particu-

\* Corresponding authors: Mi Tian, Department of Critical Care Medicine, Huashan Hospital, Fudan University, 12 Middle WuLuMuQi, Shanghai 200040, China; Ye Gong, Department of Critical Care Medicine, Huashan Hospital, Fudan University, 12 Middle WuLuMuQi, Department of Neurosurgery, Huashan Hospital, Fudan University, Shanghai 200040, China.

E-mail addresses: [mtian19@fudan.edu.cn](mailto:mtian19@fudan.edu.cn) (M. Tian), [gong\\_ye@fudan.edu.cn](mailto:gong_ye@fudan.edu.cn) (Y. Gong).

# Shuixiang Deng and Shengjie Feng contributed equally to this work.

<https://doi.org/10.1016/j.jointm.2023.08.007>

Received 6 February 2023; Received in revised form 24 June 2023; Accepted 16 August 2023

Available online 25 November 2023

Copyright © 2023 The Authors. Published by Elsevier B.V. on behalf of Chinese Medical Association. This is an open access article under the CC BY-NC-ND license (<http://creativecommons.org/licenses/by-nc-nd/4.0/>)

larly important to establish an animal model to further study the mechanism of severe ICH.

A severe ICH model should lead to drastic neuroinflammatory responses and more neuronal cell death than observed in a standard ICH model. An ideal animal model should mimic hemorrhagic stroke events, which occur naturally in human beings. Rodent, canine, feline, and primate models of ICH, using collagenase injection, microballoon insertion, or autologous blood injection, have been studied in the past.<sup>[10,11]</sup> Rats are commonly used as the experimental animals for models of ICH.<sup>[12]</sup> The method of the collagenase injection model has the advantages of simple, fast, and good repeatability. However, because the hemorrhage is mainly diffuse hemorrhage, the bleeding process is slow, and the hemorrhage focus is often mixed with normal brain tissue, which is different from clinical spontaneous ICH.<sup>[13,14]</sup> The mechanical balloon compression model can produce consistent and reproducible brain damage, but it is different from the real ICH because there are no blood components, and it cannot simulate the mechanism of blood components in the formation and development of brain injury and brain edema after ICH.<sup>[14–16]</sup> Autologous blood injection model is currently an ideal ICH model, which not only can study ICH of different degrees by controlling the amount of blood injection but also non-heparinized autologous blood injection can observe the influence of vasoactive substances released during blood coagulation on brain circulation and brain tissue, which is close to the process of clinical ICH.<sup>[14,17]</sup> It is suitable for the study of natural process and pathological characteristics of cerebral parenchymal hemorrhage, and it is an ideal model of cerebral hemorrhage. As ICH occurs mostly in the basal ganglia region in humans,<sup>[5,6]</sup> also has a basal ganglia region with a large caudate nucleus, which is easy to locate to conduct stereoscopic localization and observation in experiments. At present, although multiple studies have focused on animal models of ICH,<sup>[18]</sup> less is known about animal models of severe ICH.

This study aimed to establish a more accurate severe ICH model in rats, as well as investigate the pathological and physiological changes that occurred after ICH using imaging, histological, hematological, and behavioral tests.

## Methods

### Animals

Specific-pathogen free (SPF) 8-week to 10-week-old male Sprague-Dawley rats weighing 250–300 g were purchased from Shanghai SLAC Laboratory Animal Co., Ltd. (Shanghai, China). Animals were placed in a standard environment with a controlled temperature of 20–22 °C, humidity of 50%–60%, and a 12-h light/12-h dark cycle, accompanied by free access to food and water. This animal experiment was in accordance with the National Institutes of Health Guidelines for the Care and Use of Laboratory Animals, and was approved by the Ethics Committee of Huashan Hospital Fudan University.

### Experimental groups

After acclimatization for 1 week, a total of 120 rats were randomly divided into six groups ( $n=20$  per group) to examine the mortality rates in the first 3 days following ICH and observe their

28-day survival rate, including sham-operated (sham) group, ICH 100  $\mu\text{L}$  group, ICH 130  $\mu\text{L}$  group, ICH 160  $\mu\text{L}$  group, ICH 170  $\mu\text{L}$  group, and ICH 180  $\mu\text{L}$  group. Based on these observed mortality rates, the most suitable dose ICH groups, which best reflected the clinical mortality rate of severe ICH, were selected for the subsequent experiments.

### ICH model

The establishment of an ICH animal model was carried out using autologous blood transfusion, as previously described.<sup>[15]</sup> Briefly, rats were anesthetized by intraperitoneal injection with a mixture of ketamine (100 mg/kg) and xylazine (10 mg/kg). The depth of anesthesia was monitored by pinching the toes and tail. Rats were then immobilized with a brain stereotactic apparatus frame (David Kopf Instruments, USA) in the prone position, and a 1 mm cranial burr hole was generated. Predetermined volumes of autologous blood were collected from the lateral tail vein and slowly injected into the right basal ganglia with the coordinates of 1 mm posterior to Bregma, 3 mm lateral to the sagittal suture, and 6 mm below skull surface, at a rate of 2  $\mu\text{L}/\text{min}$ . To avoid reflux, the needle was maintained in position for an additional 10 min after partial infusion. Subsequently, the remaining portion of blood was injected into the target point again, as described above. After the injection had been completed, the needle was left in place for an additional 15 min. Then, the needle was removed slowly and the scalp was sutured. The sham group underwent the surgical procedure and received saline as the vehicle treatment.

### Assessment of short-term behavior test

Neurobehavioral tests were carried out on rats 24 h and 72 h post-ICH using the Longa method before sacrifice.<sup>[19]</sup> The neurobehavioral study was scored as previously described: 0, neurologic deficit; 1, failure to extend left forepaw fully; 2, circling to the left; 3, falling to the left; and 4, failure to walk spontaneously and loss of consciousness.

### Assessment of long-term neurological deficits

The long-term neurobehavioral outcomes were assessed by foot fault, falling latency, and Morris water maze tests.

The foot fault test was carried out to assess the placement dysfunction of the forelimbs. Rats were placed on a 0.6 cm  $\times$  1.5 cm grid surface and their paws were positioned on the wire while moving along the grid. The foot fault was defined by the slipping or falling outside the wire during movement. The frequency of foot fault was recorded within 60 s. The tests were conducted at 7 days, 14 days, and 21 days after ICH surgery.

The falling latency test was performed to assess locomotor impairment. Rats were positioned on a rotarod at a speed of 5 rounds/min. Thereafter, the rotarod speed was increased to 2 rounds/min and the time from the beginning of rotation to the falling of the rats was recorded. The tests were conducted at 7 days, 14 days, and 21 days after ICH surgery.

The Morris water maze test was performed to assess the cognitive ability of rats following ICH surgery. The experimental design included a round pool with a diameter of 110 cm and

a platform submerged 5 mm below the water surface. The water was heated to near the body temperature of the rats. Each rat was placed in the quadrant opposite to that of the platform quadrant and was allowed to search for the hidden platform. The experiment continued until all rats could find the platform within 60 s. The test was carried out on days 22–26 post-ICH surgery, and the swim distance and escape latency of each rat were recorded daily. On day 26 post-ICH, the platform was removed, and the swimming paths of all rats were observed in the water maze. The duration time of all rats in the quadrant containing the platform was recorded within 60 s.

### Measurement of brain and lung water content

The brain water content was measured in rats at 24 h and 72 h post-ICH. The cerebrum was divided into the following four areas: ipsilateral basal ganglia (Ipsi-BG), ipsilateral cortex (Ipsi-CX), contralateral basal ganglia (Cont-BG), and contralateral cortex (Cont-CX). Each part was immediately weighed on an electric analytical balance to determine the wet weight and then dried at 100 °C for 48 h to determine the dry weight. The brain water content was calculated as wet weight minus dry weight/wet weight × 100%. The lung water content was tested at 72 h post-ICH and the whole lung tissue was calculated similarly.

### Measurement of hematoma volume and hemoglobin content

After euthanasia, rat brains were perfused with phosphate buffered saline (PBS), removed, and cut into 1 mm thick slices. Brain slices were imaged with a microscope, and ImageJ software (NIH, Bethesda, MA, USA) was used to measure the hematoma size per slice. The hematoma volume (mm<sup>3</sup>) was calculated as the average area of each slice (mm<sup>2</sup>) × slice number × slice thickness (mm).

After determination of the hematoma volume, the brain slices were placed into glass dishes with 3 mL of cold PBS, and homogenized for 60 s, then sonicated for 2 min. Samples were centrifuged at 10,000 rounds/min at 4 °C for 30 min. The supernatant was incubated with Drabkin's reagent (Sigma-Aldrich, USA) at a ratio of 1:4 for 15 min. The absorbance was read at 540 nm using a spectrophotometer.

### Magnetic resonance imaging (MRI)

MRI scans were performed using a 7.0 Tesla MR scanner (BioSpec70/20USR, Bruker, Germany) 24 h after ICH. Rats were anesthetized with a mixture of ketamine (100 mg/kg) and xylazine (10 mg/kg). T2-weighted imaging (T2WI) was performed, as previously described.<sup>[20]</sup> Cube T2WI sequences were obtained with a view field of 50 mm × 50 mm, matrix 256 mm × 256 mm, and thickness of 1 mm, with a total of 15 coronal sections.

### Immunofluorescence assay

Tissues were fixed with 10% formalin for 48 h, dehydrated using a sucrose gradient of 20%–30%, embedded in optimal cutting temperature (OCT) compound, and immediately frozen at –80 °C. The frozen samples were cut into slices of 10 μm thickness using a Leica CM1950 cryostat (Leica, Germany). Samples

were then permeabilized with 0.3% Triton for 10 min, blocked with 5% donkey serum for 1 h, and incubated overnight at 4 °C with the following primary antibodies: anti-Iba-1 (1:200, Abcam, England) and anti-neuron (1:150, Abcam, England). Then, the slices were washed three times with PBS for 10 min and incubated with secondary antibodies conjugated with Alexa Fluor 488/555 (Invitrogen, Waltham, MA, USA) at room temperature in the dark. Nuclei were stained with 4',6-diamidino-2-phenylindole (DAPI), and the coverslips were mounted. Images were captured using a fluorescence microscope (Olympus, Japan).

### Histology

The lung tissues of rats were collected at 72 h post-ICH and fixed with 10% formalin at room temperature for 24 h. Subsequently, the tissues were dehydrated in an ethanol gradient, embedded in paraffin, and cut into sections at a thickness of 5 μm. Staining was carried out using hematoxylin and eosin (H&E), and morphological changes were captured under a light microscopy.

### Western blot

Total protein was extracted from the lung tissue using RIPA lysis buffer (Beyotime Institute of Biotechnology, Shanghai, China) and quantified. Protein (30 μg/lane) was then separated by 10% sodium dodecyl sulfate-polyacrylamide gel electrophoresis (SDS-PAGE) and transferred onto polyvinylidene fluoride (PVDF) membranes (Millipore, Bedford, MA, USA). After blocking with 5% skimmed milk at room temperature for 2 h, the membranes were incubated with the following primary antibodies: rabbit anti-interleukin (IL)-1β (1:1000, ab9722, Abcam) and rabbit anti-tumor necrosis factor (TNF)-α (1:1000, ab6671, Abcam) at 4 °C overnight. The membranes were then incubated with horseradish peroxidase-conjugated secondary antibodies at room temperature for 2 h. Protein bands were visualized by enhanced chemiluminescence (ECL; Beyotime Institute of Biotechnology) and quantified using ImageJ software (NIH).

### Statistical analysis

All data were analyzed using GraphPad Prism (version 8.0, GraphPad Software Inc., La Jolla, CA, USA) and presented as mean ± standard deviation (SD). Multiple comparisons were analyzed using one-way or two-way analysis of variance (ANOVA) followed by the Tukey *post hoc* test. The survival curve was assessed using the Kaplan–Meier method. All differences were considered to be statistically significant at *P* < 0.05.

## Results

### Animal mortality rate

By establishing a model of severe ICH, we found that the mortality rates in the 170 μL and 180 μL ICH groups were 75% and 100%, respectively, as shown in Figure 1A, and were therefore too high to represent the mortality of patients with clinical severe ICH, so to study the optimal dose required to establish a severe ICH model, the 100 μL, 130 μL, and 160 μL volumes

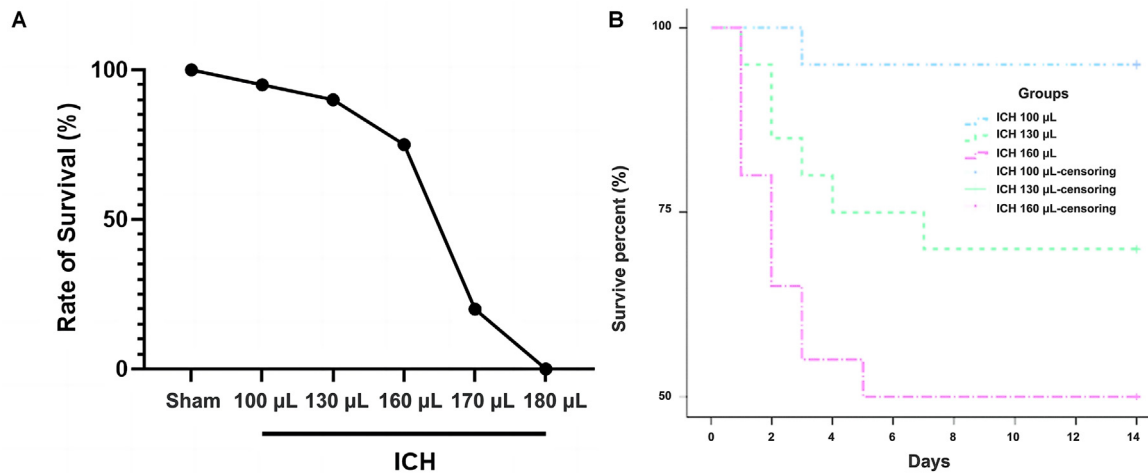


**Figure 1.** Establishment of severe ICH model with injection of different blood volumes. A: Survival rate of rats injected with different blood volumes during the first 3 days post-ICH ( $n=20$  per group). B: The 28-day survival rate after ICH by Kaplan–Meier ( $n=20$  per group). ICH: Intracerebral hemorrhage.

were selected for further survival, behavioral, and histological studies, respectively.

The mortality rate of rats increased significantly with an increased volume of autologous blood injection. The 28-day mortality rate was 5% in the ICH 100 μL group, 20% in the ICH 130 μL group, and 40% in the ICH 160 μL group. The 28-day mortality rate in the ICH 160 μL group was significantly higher than that observed in the ICH 100 μL group and was the highest overall, as shown in Figure 1B.

#### Hematoma severity after ICH

The severity of each ICH group was assessed by measuring the hematoma volume and hemoglobin content. As shown in Figure 2A–C, the hematoma volume and hemoglobin content were significantly increased in the ICH 130 μL and ICH 160 μL groups compared with the ICH 100 μL group 24 h and 72 h post-ICH ( $P < 0.05$ ) and ICH 160 μL rats exhibited elevated hematoma volumes and hemoglobin content compared to ICH 130 μL rats, indicating that the increase in autologous blood volume aggravated the severity of the hematoma. The T2WI showed no abnormalities in the sham group, while rounded or oval hematoma was observed in the right basal ganglia of the ICH groups. The ICH 160 μL group exhibited obvious perihematomal edema with high signal shadow compared to the sham and ICH 100 μL groups, as shown in Figure 2D.

#### Short-term neurobehavior and brain edema after ICH

Impairments in neurological behavior following ICH were evaluated using the Longa score 24 h and 72 h post-ICH. As shown in Figure 3A, all ICH groups had significantly higher Longa scores at both 24 h and 72 h post-ICH compared to the sham group. Markedly elevated Longa scores were observed in the ICH 130 μL and ICH 160 μL groups compared to the ICH 100 μL group, suggesting that the ICH rat model established using 130 μL or 160 μL autologous blood exhibited severe neurological behavior impairment. The degree of brain edema in each group was assessed by measuring the brain water con-

tent. As shown in Figure 3B and C, no significant difference in brain water content was observed in the Cont-BG and Cont-CX, whereas the brain water content in the Ispi-BG and Ispi-CX regions was markedly increased 24 h and 72 h post-ICH ( $P < 0.05$ ). Of note, the brain water content in the Ispi-BG and Ispi-CX regions increased with an increasing volume of autologous blood and cerebral edema became more apparent after ICH over time. Compared with the ICH 100 μL group, cerebral edema was more evident in the Cont-BG and Cont-CX of the ICH 130 μL and ICH 160 μL groups ( $P < 0.05$ ), as shown in Figure 3B,C.

#### Microglial activation and neuronal death after ICH

Immunofluorescence staining for Iba-1 as a microglial marker and neuron as a neuronal marker were carried out to examine the effects of different autologous blood volumes on microglial activation and neuronal death post-ICH. As shown in Figure 4A–C, the morphology of Iba-1-positive cells changed after ICH, with more severe morphological changes associated with higher volumes of autologous blood. The number of Iba-1-positive cells was also markedly increased in the ICH groups compared to the sham group, especially in the ICH 160 μL group. A marked reduction in neuron-positive cells was observed in ICH rats compared to sham rats, as shown in Figure 4D–F, suggesting that ICH led to neuronal death.

#### Long-term neurological deficits after ICH

To determine the effects of different autologous blood volumes on long-term neurological deficits following ICH surgery, the Morris water maze test was conducted on days 22–26 post-ICH, as well as foot fault and falling latency tests on days 7, 14, and 21 post-ICH. The Morris water maze test revealed that from the second day of testing, the swim distance and escape latency were significantly increased in ICH rats compared to sham rats, indicating that ICH rats had more severe cognitive deficits than the sham group. The ICH 130 μL and ICH 160 μL rats exhibited a higher loss of cognitive ability than the ICH 100 μL rats on the

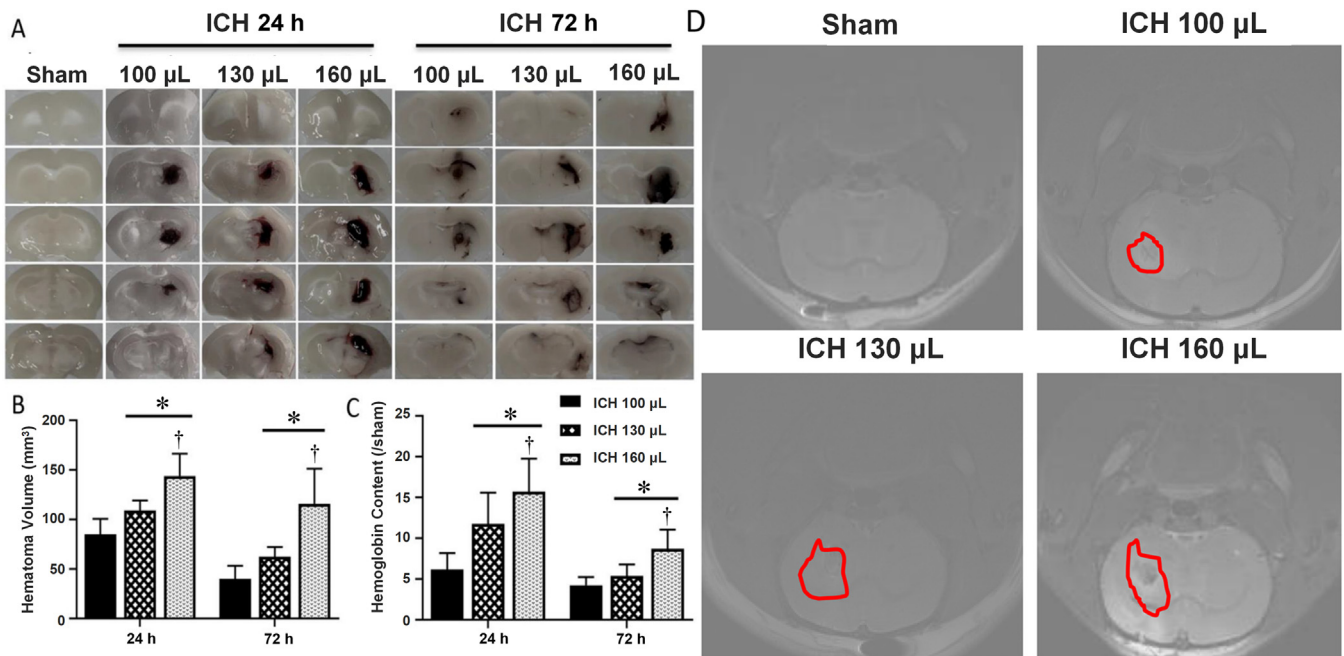


**Figure 2.** Evaluation of the severity of the ICH model. A: Representative images of the brain sections of rats 24 h and 72 h after ICH ( $n=6$  per group). B: Hematoma volume at 24 h and 72 h after ICH ( $n=6$  per group). C: Hemoglobin content at 24 h and 72 h after ICH ( $n=6$  per group). D: Representative T2-weighted MRI scans 72 h after induction of ICH using different autologous blood volumes in rats. Red circles show the areas of brain hematoma ( $n=3$  per group). \* $P < 0.05$  vs. ICH 100  $\mu\text{L}$  group. † $P < 0.05$  vs. ICH 130  $\mu\text{L}$  group. ICH: Intracerebral hemorrhage; MRI: Magnetic resonance imaging.

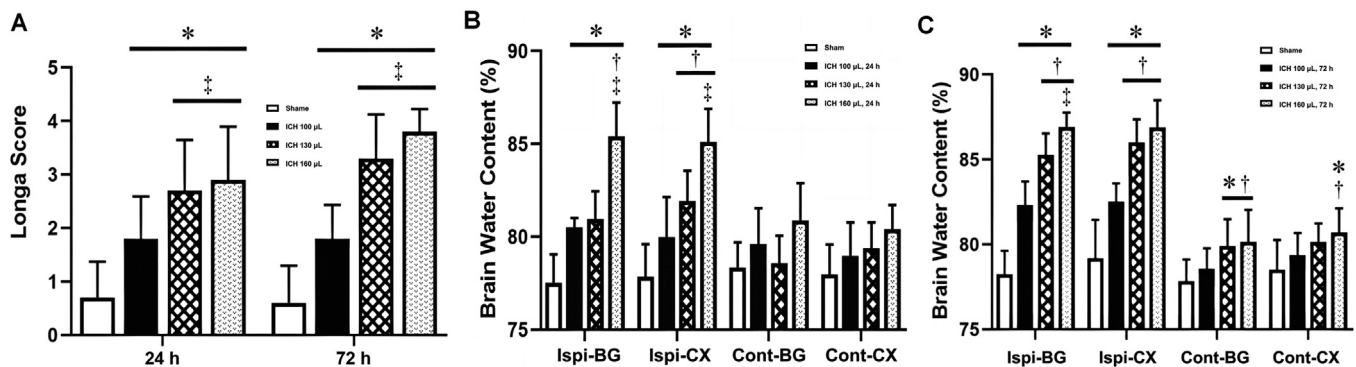


**Figure 3.** Short-term neurobehavior and brain edema after ICH. A: Short-term neurological function (Longa score) was assessed 24 h and 72 h after ICH ( $n=6$  per group). B: Brain edema was measured 24 h post-ICH ( $n=6$  per group). C: Brain edema at 72 h post-ICH ( $n=6$  per group). \* $P < 0.05$  vs. Sham group † $P < 0.05$  vs. ICH 100  $\mu\text{L}$  group; ‡ $P < 0.05$  vs. ICH 130  $\mu\text{L}$  group. Cont-BG: Contralateral basal ganglia; Cont-CX: Contralateral cortex; ICH: Intracerebral hemorrhage; Ipsi-BG: Ipsilateral basal ganglia; Ipsi-CX: Ipsilateral cortex.

third and fourth days of testing, as seen in Figure 5A and B. On the fifth day of testing, ICH rats had a lower duration time in the target quadrant than the sham rats, especially the ICH 130  $\mu\text{L}$  and ICH 160  $\mu\text{L}$  groups, as seen in Figure 5C and D, further verifying that a change in cognitive ability had occurred following ICH surgery.

Foot fault and falling latency tests were also carried out to assess the placement dysfunction of forelimbs and locomotor impairments, respectively. As shown in Figure 5E and F, compared to the sham group, ICH rats had a lower falling latency and elevated frequency of foot fault with the left forelimb. These changes were more pronounced in the ICH 130  $\mu\text{L}$  and ICH 160  $\mu\text{L}$  groups than in the ICH 100  $\mu\text{L}$  groups at days 7, 14, and 21 post-ICH. In particular, the left forelimb foot fault in the ICH 160  $\mu\text{L}$  group was significantly higher than in the ICH 130  $\mu\text{L}$  group during the day.

### Lung injury after ICH

Finally, we examined the morphology and inflammatory markers in the lung tissue after induction of ICH with different blood volumes. Histological analysis revealed that sham rats presented with normal intra-alveolar structure, but after ICH, disruption of the intra-alveolar structure was evident, with the severity increasing with higher blood volumes, as seen in Figure 6A and B. The lung injury scores indicated that most severe lung damage was associated with increased hematoma. The lung injury score was significantly higher in the ICH 160  $\mu\text{L}$  group than in the sham and ICH 100  $\mu\text{L}$  groups ( $P < 0.05$ ), as seen in Figure 6C.

The levels of TNF- $\alpha$  and IL-1 $\beta$  protein expression levels were elevated in the ICH 100  $\mu\text{L}$ , 130  $\mu\text{L}$ , and 160  $\mu\text{L}$  groups compared to the sham group. The highest levels were observed in the ICH

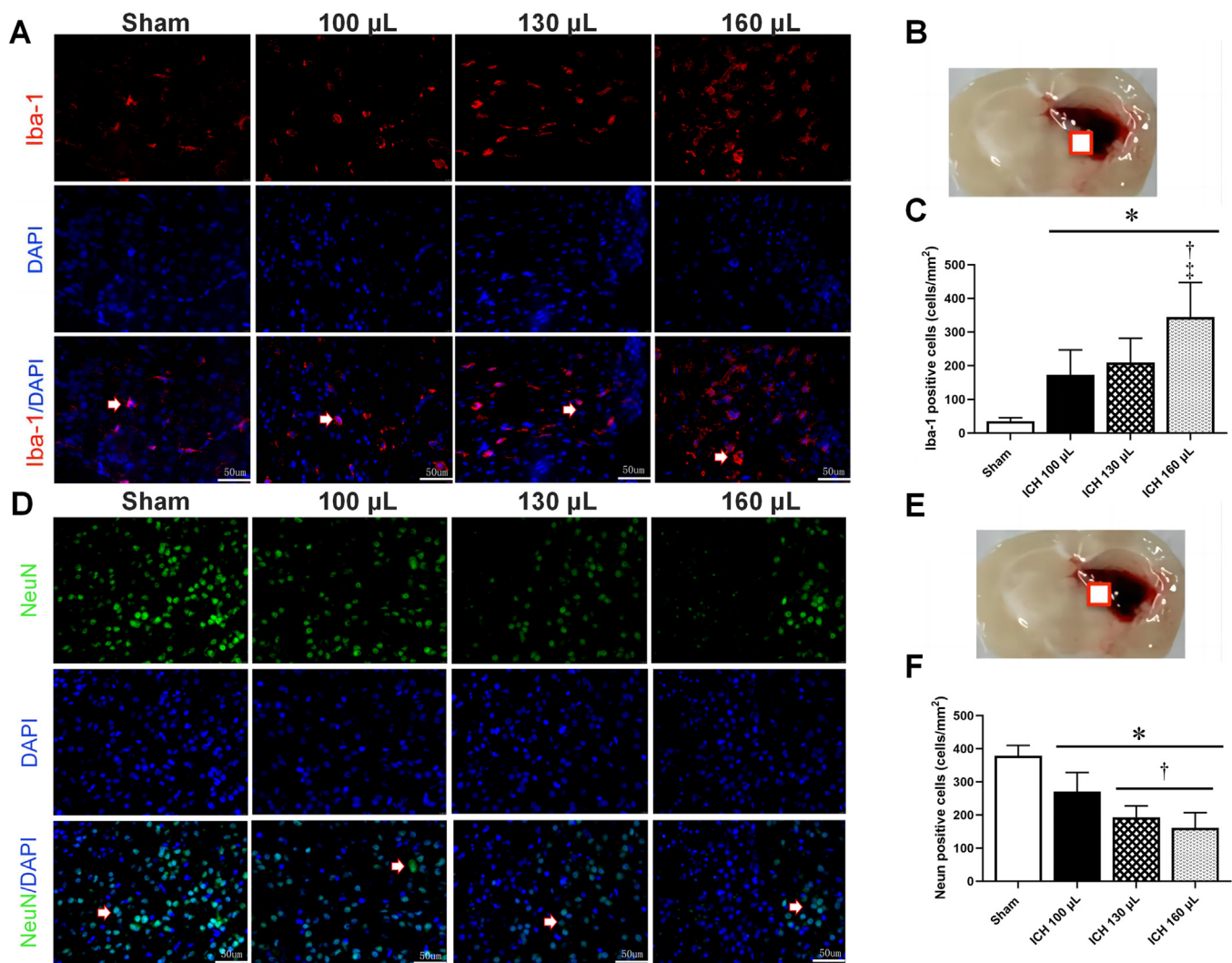


**Figure 4.** Increased blood volume exacerbates microglial activation and neuronal apoptosis post-ICH. A–C: Representative images and quantitative analysis of immunofluorescence staining of Iba-1-positive cells in the ipsilateral brain hemisphere at 72 h after ICH ( $n=4$  per group). D–F: Representative images and quantitative analysis of immunofluorescence staining of NeuN-positive cells in the ipsilateral brain hemisphere at 72 h after ICH ( $n=4$  per group). Arrow: typical positive result; square: brain tissue sampling site.

\* $P < 0.05$  vs. Sham group; † $P < 0.05$  vs. ICH 100  $\mu\text{L}$  group; ‡ $P < 0.05$  vs. ICH 130  $\mu\text{L}$  group. Scale bar=50  $\mu\text{m}$ .

DAPI: 4',6-diamidino-2-phenylindole; ICH: Intracerebral hemorrhage; NeuN: Neuron.

160  $\mu\text{L}$  group, suggesting that inflammation occurred in the lung tissue following ICH, as seen in Figure 7A and B. The increased lung water content found in ICH rats suggested that lung edema was more severe following ICH, especially in the ICH 160  $\mu\text{L}$  group, as shown in Figure 7C and D.

## Discussion

The condition of ICH is a severe public health problem that contributes to high rates of disability and mortality worldwide.<sup>[21]</sup> At present, there are still no effective therapeutic strategies for improving the clinical outcome and quality of life of patients suffering from ICH. There is therefore a critical need to construct a reproducible animal model that simulates the development of brain injury following ICH, providing a valuable tool to further the understanding of pathological mechanisms associated with ICH and to develop potential therapeutic interventions.

The autologous blood model was adopted in this study due to its ability to closely simulate clinical ICH. The autologous blood injection method not only allowed the degree of severity of ICH to be controlled but also allowed the release of vascular active substances to be observed during the blood coagulation process, which was necessary to study the natural process and pathological morphology of cerebral parenchymal hemorrhage.<sup>[14]</sup> Nath et al.<sup>[22]</sup> injected blood volumes of 25  $\mu\text{L}$ , 50  $\mu\text{L}$ , and 100  $\mu\text{L}$  into the rat brain, equivalent to 20 mL, 40 mL, and 80 mL of blood leakage in the human brain, to simulate different degrees of clinical ICH. This study established an ICH model in rats by injecting 100  $\mu\text{L}$  of blood, but the 28-day mortality rate at this volume was only 5%. This value was significantly lower than the clinical mortality rate, which ranges from 32% to 52% in the first month following ICH, while only 50% of patients independently survived 1 year after ICH.<sup>[23,24]</sup> To better reflect the clinical severity of ICH, blood volumes of 130  $\mu\text{L}$  and 160  $\mu\text{L}$  were used to construct a severe ICH rat model and the 28-day

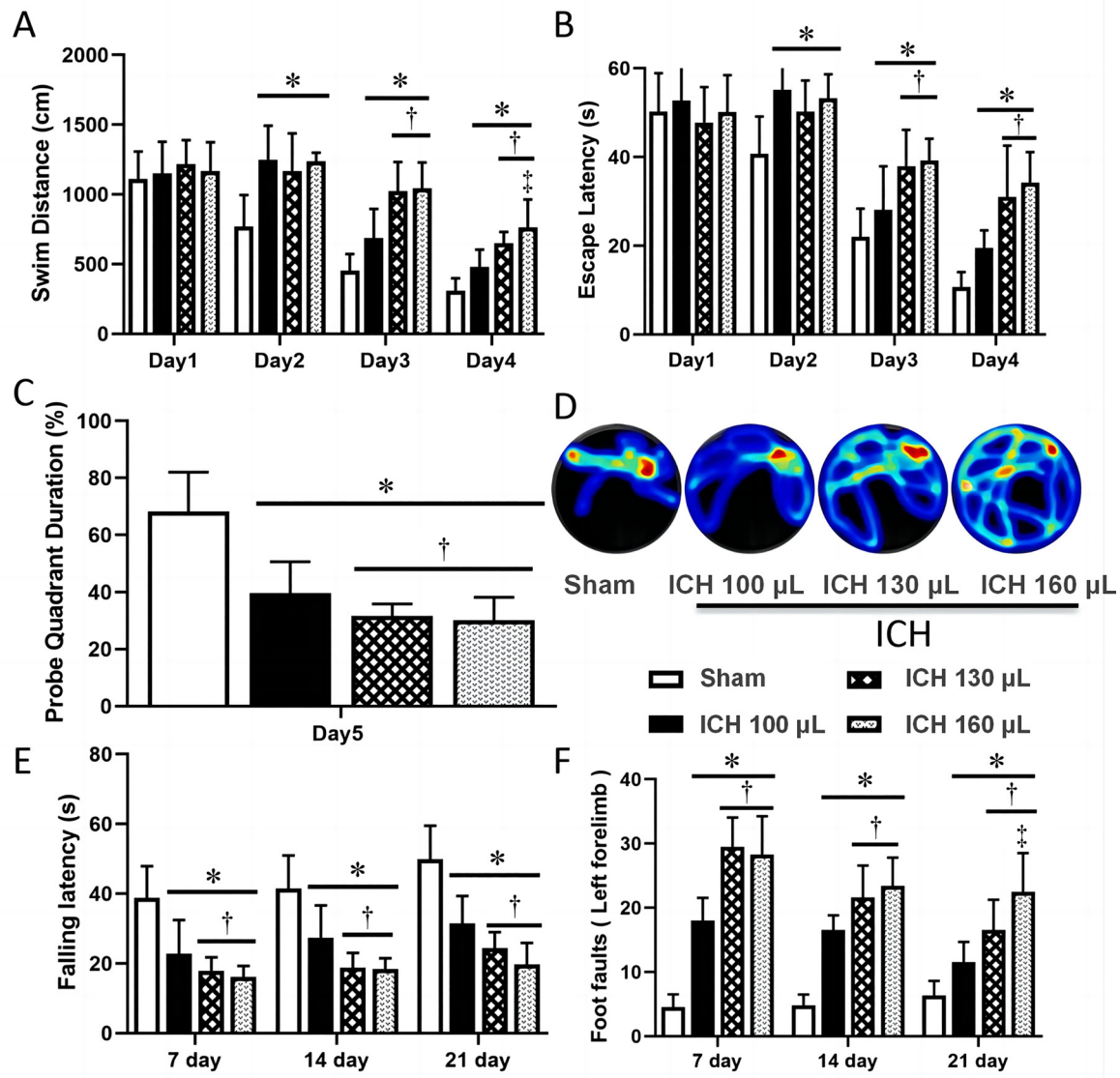


**Figure 5.** Evaluation of long-term neurological deficits in ICH models of varying severity. A: Swim distance of Morris water maze test on days 22–26 after ICH. B: Escape latency of Morris water maze test on days 22–26 after ICH. C: Probe quadrant duration of Morris water maze test on day 27. D: Typical traces of Morris water maze test on day 27 after ICH. E: Rotarod test performed on days 7, 14, and 21 post-ICH ( $n=8$  per group). F: Foot fault test performed on days 7, 14, and 21 post-ICH ( $n=8$  per group).

\* $P < 0.05$  vs. Sham group † $P < 0.05$  vs. ICH 100  $\mu\text{L}$  group; ‡ $P < 0.05$  vs. ICH 130  $\mu\text{L}$  group.

ICH: Intracerebral hemorrhage.

mortality rate after ICH increased with an increasing blood volume injection. Since an injection of 160  $\mu\text{L}$  of blood led to a high 28-day mortality (40%), this volume was used to establish a severe ICH rat model.

Hematoma volume has been recognized as an independent predictor of poor functional outcome and clinical mortality of ICH patients, and the risk of neurological deterioration increases with hematoma growth.<sup>[25,26]</sup> Previous studies have suggested that the primary injury in response to hematoma expansion and hemoglobin production contributed to a cascade of events triggering secondary injury, which is responsible for the poor outcome after ICH.<sup>[27–29]</sup> Activation of microglia and hematoma-induced neuronal death in the surrounding parenchymal rim has also been considered to be important targets that contribute to brain damage.<sup>[30,31]</sup> In addition, an increasing number of clin-

ical studies have found that systemic inflammatory response syndrome and ICH-associated complications accentuated brain injury and jeopardized clinical outcomes.<sup>[32–34]</sup> Multiple studies focusing on the autologous blood injection-induced ICH rat model have reported severe brain edema and behavioral disorders in ICH rats, as well as microglial activation and neuronal death in the perihematomal area.<sup>[35–37]</sup> It is worth noting that although the cortex and hippocampus are not *in situ* hemorrhagic foci, hematoma-induced secondary injury, such as neuronal death in the cortex and hippocampus, may be partially responsible for cognitive deficits associated with ICH.<sup>[36,38]</sup> This study found more severe brain edema, hematoma expansion, microglial activation, neuronal death, and neurological deficits after ICH surgery with injections of 130  $\mu\text{L}$  and 160  $\mu\text{L}$  autologous blood volumes than after 100  $\mu\text{L}$ , suggest-

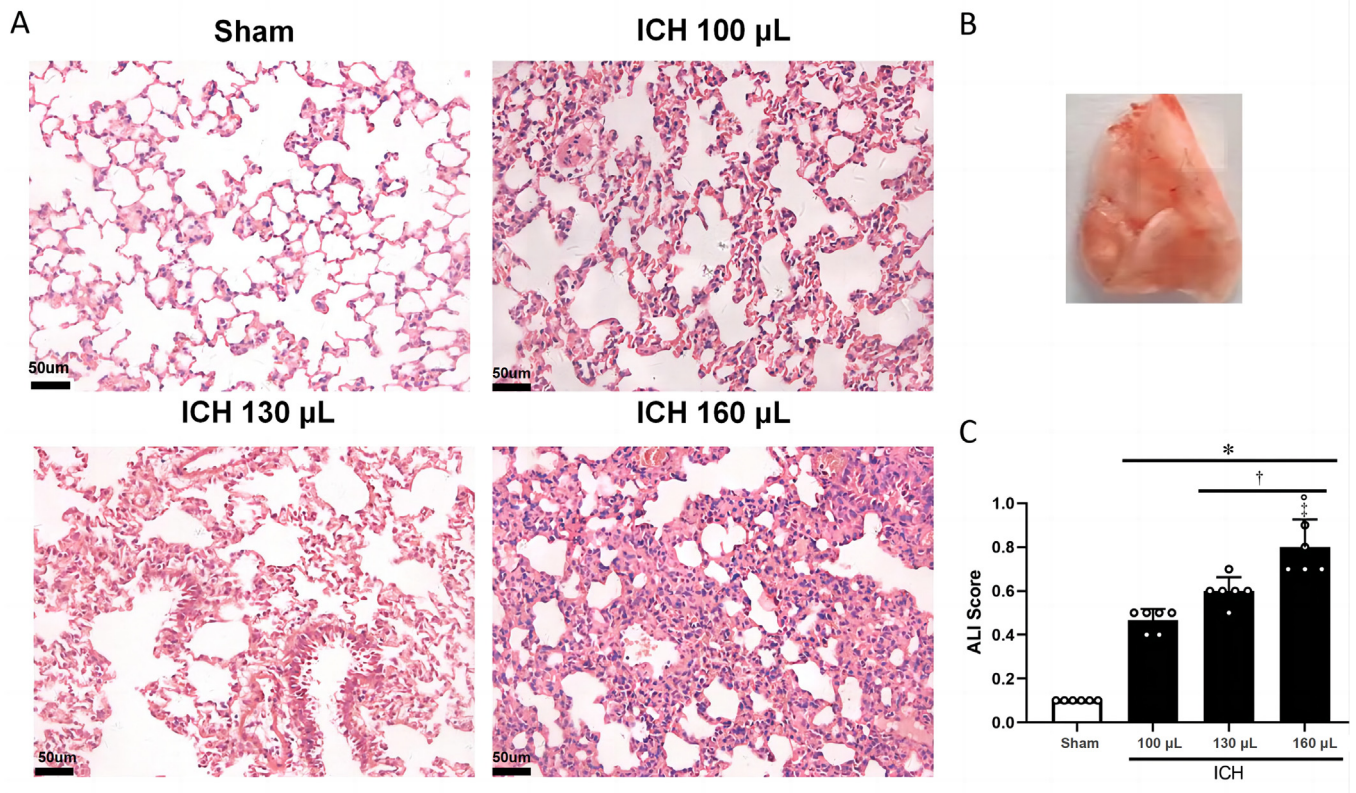


**Figure 6.** Histological assessment of lung injury in ICH models of varying severity. A: Representative H&E staining images of the lung tissue obtained from rats in the indicated groups. B: The lung slice on the right of the top panel indicates the location of the staining quantification. C: Total ALI scores from the indicated groups ( $n=6$  per group).

\* $P < 0.05$  vs. Sham group † $P < 0.05$  vs. ICH 100 μL group; ‡ $P < 0.05$  vs. ICH 130 μL group.  
ALI: Acute lung injury; H&E: Hematoxylin and eosin; ICH: Intracerebral hemorrhage.

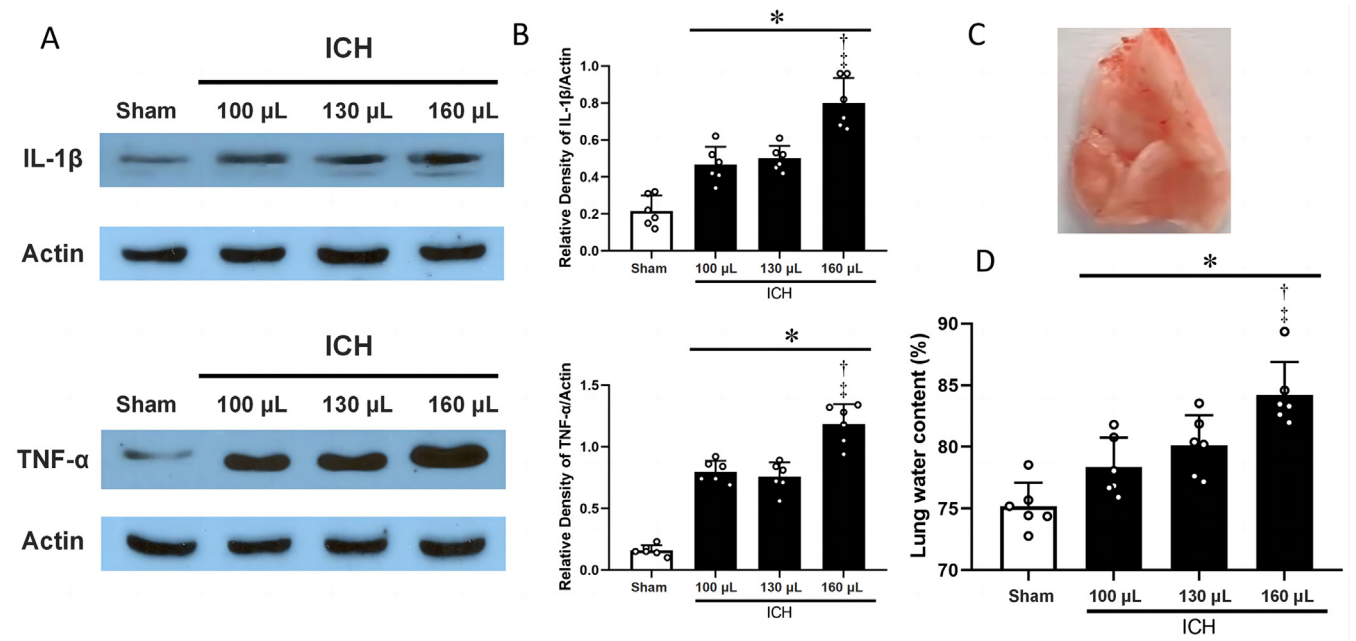


**Figure 7.** Lung inflammation and edema assessment of lung injury in ICH models of varying severity. A: Representative western blots of TNF- $\alpha$  and IL-1 $\beta$  protein levels at 72 h after ICH. B: Quantitative analyses of TNF- $\alpha$  and IL-1 $\beta$  protein levels at 72 h after ICH. C: The lung slice on the right of the top panel indicates the location of the staining quantification. D: Lung edema at 72 h post-ICH.

\* $P < 0.05$  vs. Sham group † $P < 0.05$  vs. ICH 100 μL group; ‡ $P < 0.05$  vs. ICH 130 μL group.  $n=6$  per group.  
ICH: Intracerebral hemorrhage; IL: Interleukin; TNF: Tumor necrosis factor.

ing that an increased autologous blood volume resulted in more severe ICH.

Finally, in addition to parenchymal hematoma formation and brain injury, ICH-induced high intracranial pressure may trigger the localized activation of coagulation and the immune system, releasing cytokines both locally and spreading to other tissues. One study estimated that approximately 23%–58% of ICH patients developed infection complications, such as pneumonia,<sup>[39]</sup> while Elmer et al.<sup>[40]</sup> reported that the prevalence of acute respiratory distress syndrome (ARDS) after clinical spontaneous ICH was as high as 27%. A study by Wu et al.<sup>[41]</sup> observed enhanced lung inflammation in an experimental ICH rat model induced by stereotaxic intrastriatal administration of bacterial collagenase and showed that ICH promoted the production of pro-inflammatory cytokines in brain and lung tissues, accompanied by pulmonary damage. The present study also examined the morphology and inflammatory markers in the lung tissue after ICH surgery and found that, compared to the sham, the lung tissues of ICH rats showed disruption of the intra-alveolar structure and high expression levels of TNF- $\alpha$  and IL-1 $\beta$ , as well as severe lung edema, indicating that ICH resulted in lung injury, especially when injected with a blood volume of 160  $\mu$ L.

There were several limitations in the present study. Only a single autologous blood ICH model was selected and a collagenase model was not used to observe the pathophysiological mechanism of severe ICH. Emerging evidence has indicated ICH induces more severe brain injury in aged male animals than young females, but only 8-week-old male adult Sprague-Dawley rats were used in the present study. Further studies are required to examine the pathophysiological mechanism of severe ICH in different age groups and female animals. Finally, the long-term histopathological changes in different hematoma groups were not recorded so this should be the focus of future studies.

## Conclusions

An optimal 160  $\mu$ L autologous blood injection-induced ICH rat model was established to simulate severe ICH and it provided a valuable tool to examine the pathological mechanisms and develop potential therapeutic intervention strategies for severe ICH.

## Author Contributions

**Ye Gong** developed the study design and coordinated its implementation. **Mi Tian** participated in guiding the study design. **Shuixiang Deng** and **Shengjie Feng** contributed equally to this manuscript and wrote the main manuscript text. **Yuewen Xin** and **Yu He** aided in the preparation of the manuscript. **Yao Wang** prepared Figures 1–6. All authors reviewed the manuscript.

## Acknowledgment

None.

## Funding

This study was supported by a grant from the **Shanghai Hospital Development Center (SHDC2020CR3021A to YG)**, the

**Science and Technology Commission of Shanghai Municipality (21ZR1410700 to S.D.)**, and the **National Natural Science Foundation of China (82101536 to S.D.)**.

## Ethics Statement

This animal experiment was in accordance with the National Institutes of Health Guidelines for the Care and Use of Laboratory Animals, and was approved by the Ethics Committee of Huashan Hospital Fudan University (Review number: 201802035S).

## Conflict of Interest

The authors declare that they have no known competing financial interests or personal relationships that could have appeared to influence the work reported in this paper.

## Data Availability

The datasets used or analyzed during the current study are available from the corresponding author on reasonable request.

## References

- [1] GBD 2019 Stroke Collaborators. Global, regional, and national burden of stroke and its risk factors, 1990–2019: a systematic analysis for the Global Burden of Disease Study 2019. *Lancet Neurol* 2021;20(10):795–820. doi:10.1016/s1474-4422(21)00252-0.
- [2] Jolink WMT, van Veluw SJ, Zwanenburg JJM, Rozemuller AJM, van Hecke W, Frosch MP, et al. Histopathology of cerebral microinfarcts and microbleeds in spontaneous intracerebral hemorrhage. *Transl Stroke Res* 2022;14(2):174–84. doi:10.1007/s12975-022-01016-5.
- [3] Sacco S, Marini C, Toni D, Olivieri L, Carolei A. Incidence and 10-year survival of intracerebral hemorrhage in a population-based registry. *Stroke* 2009;40(2):394–9. doi:10.1161/STROKEAHA.108.523209.
- [4] van Asch CJ, Luitse MJ, Rinkel GJ, van der Tweel I, Algra A, Klijn CJ. Incidence, case fatality, and functional outcome of intracerebral haemorrhage over time, according to age, sex, and ethnic origin: a systematic review and meta-analysis. *Lancet Neurol* 2010;9(2):167–76. doi:10.1016/S1474-4422(09)70340-0.
- [5] Mark SG. *Handbook of neurosurgery*, 87; 2016. p. 1331–2.
- [6] RA P. *Neuropathology*, 2; 2012. p. 49–50.
- [7] Mu S, Lin Y, Xu Y, Wei X, Zeng Z, Lin K, et al. A novel rat model for cerebral venous sinus thrombosis: verification of similarity to human disease via clinical analysis and experimental validation. *J Transl Med* 2022;20(1):174. doi:10.1186/s12967-022-03374-y.
- [8] Yokoyama T, Koba T, Kaneko M. [Motor weakness in the lateral type of hypertensive intracerebral hemorrhage. On the mechanism of the dissociation of motor weakness between arm and leg (author's transl)]. *No To Shinkei* 1978;30(1):55–9.
- [9] Poon MT, Fonville AF, Al-Shahi Salman R. Long-term prognosis after intracerebral haemorrhage: systematic review and meta-analysis. *J Neurol Neurosurg Psychiatry* 2014;85(6):660–7. doi:10.1136/jnnp-2013-306476.
- [10] Leonardo CC, Robbins S, Doré S. Translating basic science research to clinical application: models and strategies for intracerebral hemorrhage. *Front Neurol* 2012;3:85. doi:10.3389/fneur.2012.00085.
- [11] Krafft PR, Bailey EL, Lekic T, Roland WB, Altay O, Tang J, et al. Etiology of stroke and choice of models. *Int J Stroke* 2012;7(5):398–406. doi:10.1111/j.1747-4949.2012.00838.x.
- [12] MacLellan CL, Silasi G, Auriat AM, Colbourne F. Rodent models of intracerebral hemorrhage. *Stroke* 2010;41(10 Suppl):S95–8. doi:10.1161/strokeaha.110.594457.
- [13] James ML, Warner DS, Laskowitz DT. Preclinical models of intracerebral hemorrhage: a translational perspective. *Neurocrit Care* 2008;9(1):139–52. doi:10.1007/s12028-007-9030-2.
- [14] Manaenko A, Chen H, Zhang JH, Tang J. Comparison of different preclinical models of intracerebral hemorrhage. *Acta Neurochir Suppl* 2011;111:9–14. doi:10.1007/978-3-7091-0693-8\_2.
- [15] Rynkowski MA, Kim GH, Komotar RJ, Otten ML, Ducruet AF, Zacharia BE, et al. A mouse model of intracerebral hemorrhage using autologous blood infusion. *Nat Protoc* 2008;3(1):122–8. doi:10.1038/nprot.2007.513.
- [16] Lopez Valdes E, Hernandez Lain A, Calandre L, Grau M, Cabello A, Gomez-Escalonilla C. Time window for clinical effectiveness of mass evacuation in a rat balloon model mimicking an intraparenchymatous hematoma. *J Neurol Sci* 2000;174(1):40–6. doi:10.1016/S0022-510X(99)00288-9.
- [17] Rosenberg GA, Mun-Bryce S, Wesley M, Kornfeld M. Collagenase-induced intracerebral hemorrhage in rats. *Stroke* 1990;21(5):801–7. doi:10.1161/01.STR.21.5.801.

- [18] Jia P, He J, Li Z, Wang J, Jia L, Hao R, et al. Profiling of blood-brain barrier disruption in mouse intracerebral hemorrhage models: collagenase injection vs. autologous arterial whole blood infusion. *Front Cell Neurosci* 2021;15:699736. doi:10.3389/fn-cel.2021.699736.
- [19] Longa EZ, Weinstein PR, Carlson S, Cummins R. Reversible middle cerebral artery occlusion without craniectomy in rats. *Stroke* 1989;20(1):84–91. doi:10.1161/01.STR.20.1.84.
- [20] Ye F, Hua Y, Keep RF, Xi G, Garton HJL. CD47 blocking antibody accelerates hematoma clearance and alleviates hydrocephalus after experimental intraventricular hemorrhage. *Neurobiol Dis* 2021;155:105384. doi:10.1016/j.nbd.2021.105384.
- [21] Chen HS, Hsieh CF, Chau TT, Yang CD, Chen YW. Risk factors of in-hospital mortality of intracerebral hemorrhage and comparison of ICH scores in a Taiwanese population. *Eur Neurol* 2011;66(1):59–63. doi:10.1159/000328787.
- [22] Nath FP, Jenkins A, Mendelow AD, Graham DI, Teasdale GM. Early hemodynamic changes in experimental intracerebral hemorrhage. *J Neurosurg* 1986;65(5):697–703. doi:10.3171/jns.1986.65.5.0697.
- [23] Adeoye O, Broderick JP. Advances in the management of intracerebral hemorrhage. *Nat Rev Neurol* 2010;6(11):593–601. doi:10.1038/nrneurol.2010.146.
- [24] Gareev I, Yang G, Sun J, Beylerli O, Chen X, Zhang D, et al. Circulating microRNAs as potential noninvasive biomarkers of spontaneous intracerebral hemorrhage. *World Neurosurg* 2020;133:e369–75. doi:10.1016/j.wneu.2019.09.016.
- [25] Davis SM, Broderick J, Hennerici M, Brun NC, Dinger MN, Mayer SA, et al. Hematoma growth is a determinant of mortality and poor outcome after intracerebral hemorrhage. *Neurology* 2006;66(8):1175–81. doi:10.1212/01.wnl.0000208408.98482.99.
- [26] Leira R, Dávalos A, Silva Y, Gil-Peralta A, Tejada J, Garcia M, et al. Early neurologic deterioration in intracerebral hemorrhage: predictors and associated factors. *Neurology* 2004;63(3):461–7. doi:10.1212/01.wnl.0000133204.81153.ac.
- [27] Hemphill JC 3rd, Greenberg SM, Anderson CS, Becker K, Bendok BR, Cushman M, et al. Guidelines for the management of spontaneous intracerebral hemorrhage: a guideline for healthcare professionals from the American Heart Association/American Stroke Association. *Stroke* 2015;46(7):2032–60. doi:10.1161/STR.0000000000000069.
- [28] Zhu H, Wang Z, Yu J, Yang X, He F, Liu Z, et al. Role and mechanisms of cytokines in the secondary brain injury after intracerebral hemorrhage. *Prog Neurobiol* 2019;178:101610. doi:10.1016/j.pneurobio.2019.03.003.
- [29] Guo G, Pan C, Guo W, Bai S, Nie H, Feng Y, et al. Efficacy and safety of four interventions for spontaneous supratentorial intracerebral hemorrhage: a network meta-analysis. *J Neurointerv Surg* 2020;12(6):598–604. doi:10.1136/neurintsurg-2019-015362.
- [30] Wang J, Tsirka SE. Tuftsin fragment 1-3 is beneficial when delivered after the induction of intracerebral hemorrhage. *Stroke* 2005;36(3):613–18. doi:10.1161/01.STR.0000155729.12931.8f.
- [31] Felberg RA, Grotta JC, Shirzadi AL, Strong R, Narayana P, Hill-Felberg SJ, et al. Cell death in experimental intracerebral hemorrhage: the “black hole” model of hemorrhagic damage. *Ann Neurol* 2002;51(4):517–24. doi:10.1002/ana.10160.
- [32] Hagen M, Sembill JA, Sprügel MI, Gerner ST, Madžar D, Lücking H, et al. Systemic inflammatory response syndrome and long-term outcome after intracerebral hemorrhage. *Neurol Neuroimmunol Neuroinflamm* 2019;6(5):e588. doi:10.1212/NXI.0000000000000588.
- [33] Balami JS, Buchan AM. Complications of intracerebral haemorrhage. *Lancet Neurol* 2012;11(1):101–18. doi:10.1016/S1474-4422(11)70264-2.
- [34] Zhang Y, Wang Y, Ji R, Wang A, Wang Y, Yang Z, et al. In-hospital complications affect short-term and long-term mortality in ICH: a prospective cohort study. *Stroke Vasc Neurol* 2021;6(2):201–6. doi:10.1136/svn-2020-000386.
- [35] Wang Z, Zhou F, Dou Y, Tian X, Liu C, Li H, et al. Melatonin alleviates intracerebral hemorrhage-induced secondary brain injury in rats via suppressing apoptosis, inflammation, oxidative stress, DNA damage, and mitochondria injury. *Transl Stroke Res* 2018;9(1):74–91. doi:10.1007/s12975-017-0559-x.
- [36] Gong Y, Zhang G, Li B, Cao C, Cao D, Li X, et al. BMAL1 attenuates intracerebral hemorrhage-induced secondary brain injury in rats by regulating the Nrf2 signaling pathway. *Ann Transl Med* 2021;9(21):1617. doi:10.21037/atm-21-1863.
- [37] Chen Z, Zhang H, Zhou J, Stone C, Ding Y, Zhang Y, et al. CORM-2 inhibits intracerebral hemorrhage-mediated inflammation. *Neurol Res* 2021;43(10):846–53. doi:10.1080/01616412.2021.1939484.
- [38] Aronowski J, Zhao X. Molecular pathophysiology of cerebral hemorrhage: secondary brain injury. *Stroke* 2011;42(6):1781–6. doi:10.1161/STROKEAHA.110.596718.
- [39] Lindner A, Kofler M, Rass V, Ianosi B, Gaasch M, Schiefecker AJ, et al. Early predictors for infectious complications in patients with spontaneous intracerebral hemorrhage and their impact on outcome. *Front Neurol* 2019;10:817. doi:10.3389/fneur.2019.00817.
- [40] Elmer J, Hou P, Wilcox SR, Chang Y, Schreiber H, Okechukwu I, et al. Acute respiratory distress syndrome after spontaneous intracerebral hemorrhage\*. *Crit Care Med* 2013;41(8):1992–2001. doi:10.1097/CCM.0b013e31828a3f4d.
- [41] Wu S, Fang CX, Kim J, Ren J. Enhanced pulmonary inflammation following experimental intracerebral hemorrhage. *Exp Neurol* 2006;200(1):245–9. doi:10.1016/j.expneurol.2006.01.027.